Chemical Engineering Journal 147 (2009) 150–160

Contents lists available at ScienceDirect

Chemical Engineering Journal

journal homepage: www.elsevier.com/locate/cej

Biosorption of hexacyanoferrate(III) complex anion to dead biomass of the basidiomycete *Pleurotus mutilus*: Biosorbent characterization and batch experiments

Abdelmalek Chergui[a,*], Rabah Kerbachi[a], Guy-Alain Junter[b]

[a] *Ecole Nationale Polytechnique, Département Génie de l'Environnement, 10 Avenue Hassen Badi, BP 182, El Harrach, Alger, Algeria*
[b] *Université de Rouen, Laboratoire Polymères, Biopolymères, Surfaces, CNRS FRE 3101, F76821 Mont-Saint-Aignan Cedex, France*

ARTICLE INFO

Article history:
Received 30 October 2007
Received in revised form 5 June 2008
Accepted 28 June 2008

Keywords:
Equilibrium modelling
Fungal biosorbent
Pleurotus mutilus
Iron(III)–cyanide ions
Kinetic modelling
Potentiometric titration

ABSTRACT

This work is a contribution to the use of natural, cost-effective biosorbants in industrial wastewater treatment processes, addressing more particularly to the effluents resulting from surface treatment and mining industries. A dead fungal biomass (i.e., *Pleurotus mutilus*) collected as a waste from an antibiotic production plant was tested as a biosorbent for iron(III)–cyanide complex ions. A physicochemical characterization of this biomass was followed by batch biosorption experiments. Potentiometric titration confirmed by FTIR analysis indicated a variety of functionalities on the biomass surface, primarily carboxylic and amine groups which conferred to the biosorbent a positive charge in acid medium and a negative charge in alkaline medium. Biomass pre-treatment with acetic acid slightly improved its biosorption efficiency which was also affected by the initial pH of the test solution, the size and concentration of biosorbent particles, and the stirring speed of the particle suspension. In particular, the best performance was obtained at strongly alkaline pH (around 12) even though the overall electrical charge of the biomass was negative in this pH range. The sorption kinetics obeyed both pseudo-first-order and pseudo-second-order models and intraparticle diffusion was the main limiting step in the biosorption kinetics. Applying the Langmuir isotherm modelling, the highest biosorption efficiency, i.e., the maximum solid phase concentration of complex ions (forming a complete monolayer coverage on the sorbent surface) was over 620 mg g^{-1}. Continuous fixed-bed sorption–desorption experiments are in progress to confirm these promising results.

1. Introduction

Several industries, e.g., mining and surface treatment industries, generate huge quantities of cyanides, as free ions or complexes, together with heavy metals such as nickel, copper, zinc and iron. The presence of free cyanide in waste effluents represents a real environmental danger because of the toxicity of this compound which inhibits dioxygen transfer from blood to tissues. Cyanide, strongly reactive, readily forms with metals complexes of varying stability and toxicity, for instance iron(II)– and iron(III)–cyanide complex ions. As a rule, cyanide complexes are less toxic than free ions but can be slowly decomposed under sunlight UV radiations to release free cyanide [1,2]. Strict environmental regulations are applied to waters containing free cyanide and metal cyanide complexes. In general, these waters can be released into the environment only after detoxification [2,3].

In addition to thermal treatment methods, physical, chemical and biological processes can be applied to the treatment of cyanide-loaded wastewaters. Physical and chemical treatment technologies include activated carbon adsorption, ion exchange, flotation, precipitation, chemical oxidation (by SO_2/air mixtures, hydrogen peroxide, peroxymonosulfuric acid, ozone and ultraviolet radiation, etc.), alkaline chlorination [4,5]. All these methods suffer from limitations since they often involve high capital and operational costs and may also be associated with the generation of secondary wastes presenting treatment problems.

The biological treatment of cyanide-containing effluents [6,7] is based on the ability displayed by a number of microorganisms, i.e., bacteria [8–10], fungi [11–13] and microalgae [14], to degrade cyanide or/and its metal complexes into products that are less toxic to the environment. Cyanide or metal cyanide complex ions are the sole source of nitrogen provided to microbial cultures and are degraded as cometabolic secondary substrate in the presence of a carbon source, e.g., glucose. The toxicity of cyanide and its complexes requiring the use of acclimated strains and extended incubation periods, the need for careful control and monitoring of

* Corresponding author. Tel.: +213 21 52 25 28; fax: +213 21 52 29 73.
E-mail address: a_chergui@yahoo.fr (A. Chergui).

1385-8947/$ – see front matter © 2008 Elsevier B.V. All rights reserved.
doi:10.1016/j.cej.2008.06.029

Nomenclature

b	Langmuir isotherm constant ($dm^3\ mg^{-1}$)
C_0	initial solute concentration in liquid phase ($mg\ dm^{-3}$)
C_e	liquid phase solute concentration at equilibrium ($mg\ dm^{-3}$)
C_{st}	liquid phase concentration of solute at the biosorbent surface at time t ($mg\ dm^{-3}$)
C_t	solute concentration in bulk liquid phase at time t ($mg\ dm^{-3}$)
D_i	average diffusion coefficient in the solid ($m^2\ s^{-1}$)
d_p	mean biomass particle diameter (μm)
k_1	rate constant of pseudo-first-order sorption (min^{-1})
k_2	rate constant of pseudo-second-order sorption ($g\ mg^{-1}\ min^{-1}$)
K_a	acidity constant
K_F	Freundlich isotherm constant ($mg^{(n-1)/n}\ dm^{3/n}\ g^{-1}$)
k_i	intraparticle diffusion rate constant ($mg\ g^{-1}\ s^{-0.5}$)
k_L	external (liquid-film) mass transfer coefficient ($m\ s^{-1}$)
m	mass of adsorbent used (g)
n	Freundlich isotherm exponent
q_e	solid phase concentration of adsorbate at equilibrium ($mg\ g^{-1}$)
q_m	maximum adsorption capacity of biosorbent according to Langmuir model ($mg\ g^{-1}$)
q_t	solid phase concentration of adsorbate at time t ($mg\ g^{-1}$)
R	correlation coefficient
S	surface area of the biomass per unit solution volume ($m^2\ m^{-3}$)
S_p	specific surface area of the biomass ($m^2\ g^{-1}$)
t	time (min)
V_{sol}	solution volume in biosorption tests (dm^3)
X	biomass concentration ($g\ dm^{-3}$)
ρ_{app}	apparent density of the biomass ($g\ cm^{-3}$)

biodegradation conditions (temperature, pH, aeration)—in particular the need to perform biodegradation assays at pH values that do not affect microbial activity, i.e., around neutrality, with the risk of cyanide loss as HCN, are some of the problems encountered by this promising biodegradation route. The assimilation of iron cyanide complex ions by plants fed with spiked solutions [15], the uptake of cyanide by plant tissues (leaves and roots) [16] have also been investigated. The results show that plant biomass may be a suitable candidate material for cyanide removal but need to be confirmed to assess the potentialities of these phytoremediation processes.

The special surface properties of microorganisms and plants enable them to adsorb different types of pollutants from solutions. Cell walls of microbial and plant biomasses are composed primarily of various organic compounds such as chitin, polysaccharides, lipids, amino acids, glucanes and other cellular components capable to achieve the passive uptake of different pollutants by adsorption, ion exchange, micro-precipitation, complexation or chelation. This passive bioaccumulation process (biosorption) has distinct advantages compared to the conventional methods: it does not produce other dangerous products (not polluting), it can be strongly selective and efficient and consequently profitable for the treatment of large volumes of wastewater containing low pollutant concentrations. Furthermore, cost-effective adsorbents can be obtained from biomass. Biosorption has been widely applied to wastewater treatment over a score of years, more particularly for the removal of heavy metal ions from industrial effluents [17–20]. Few studies focused on biosorption of metal–cyanide complex ions [21,22], however.

A variety of biomass is used by the SAIDAL antibiotic complex at Medea, Algeria, among which the basidomycete *Pleurotus mutilus* (*Clitopilus scyphoides*), an edible mushroom from which the tricyclic diterpenoid compound pleuromutilin, an antibiotic for veterinary use, is isolated. Huge quantities of residual *P. mutilus* biomass resulting from the antibiotic extraction process are disposed of after incineration. The purpose of the present work is to validate the valorization of this waste biomass as a biosorbent for iron(III)–cyanide ions.

The ability of a biosorbent to accumulate a given pollutant is controlled by the physical and chemical properties of both the biosorbent (size and charge of particles, functional chemical groups) and the adsorbing species (ion size and charge), together with the operating conditions of the sorption process (pH, temperature, stirring speed, ionic strength). Hence, the physical and chemical characteristics of crude and pre-treated *P. mutilus* biomass were first investigated. Batch biosorption tests were then performed under varying operating conditions to optimize the biosorption efficiency of the mycelial biomass. Finally, the sorption data were compared with standard kinetic and equilibrium models to clarify the mechanisms that control complex ion biosorption.

2. Materials and methods

2.1. Biomass preparation and characterization

2.1.1. Biomass preparation

Waste *P. mutilus* biomass was collected at the SAIDAL antibiotic production complex in Medea (Algeria). The crude biomass was washed thoroughly first with tap water, then with distilled water, and dried for 24 h at 60 °C in an oven. The dried biomass was ground manually in a mortar and sieved into seven particle size ranges: 50–80, 100–160, 160–200, 200–250, 250–315, 315–400, 400–500 μm. To try to release adsorption sites on the biosorbent surface, biomass samples were submitted to chemical treatment by soaking and shaking in acid (0.1 mol dm^{-3} HCl or 0.1 mol dm^{-3} CH_3COOH) or basic (0.1 mol dm^{-3} NaOH) solutions. All biomass fractions were stocked at room temperature before characterization and biosorption experiments.

2.1.2. Biomass characterization

2.1.2.1. Acid–base potentiometric titration. A mass of 1.25 g of fungal biomass was added to 125 cm^3 of 0.05 mol dm^{-3} NaCl solution in an Erlenmeyer flask equipped with magnetic stirring. Precise volumes of 0.1 mol dm^{-3} HCl or 0.01 mol dm^{-3} NaOH were added to the biomass suspension. After each addition of titrant, the suspension was agitated (150 rpm) for 12 h, ensuring pH stabilization. pH was measured using a HI 221 pH-meter (Hanna Instruments, Tanneries, France) equipped with a HI 1131P glass electrode (Hanna).

The overall biomass charge per unit surface was calculated as follows considering electrical neutrality of the liquid-biomass suspension:

- acid pH (HCl added):

$$Q_x^+ = \frac{F(V_0 + V_a)}{mS_p}\left(\frac{N_a V_a}{V_0 + V_a} + [OH^-] - [H^+]\right) \quad (1)$$

where Q_x^+ is the positive overall charge per unit surface of biomass, V_0 is the initial volume of liquid medium in the test flask, N_a and V_a are the normality and the added volume of acid, respectively, m and S_p are the mass and specific surface area of

the biomass, respectively, $[H^+]$ and $[OH^-]$, the molar concentrations of protons and hydroxyl ions in solution, respectively, and F the Faraday constant.

- basic pH (NaOH added):

$$Q_x^- = \frac{F(V_0 + V_b)}{mS_p}\left(\frac{N_b V_b}{V_0 + V_b} + [H^+] - [OH^-]\right) \quad (2)$$

in which Q_x^- is the negative overall charge per unit surface of biomass, and N_b and V_b are the normality and added volume of base, respectively.

2.1.2.2. Zeta potential. The zeta potential of biomass particles was measured using a Nano-ZS Zetasizer from Malvern (Malvern, UK).

2.1.2.3. IR spectral analysis. Translucent sample disks were prepared by encapsulating 1 mg of finely ground biomass particles in 300 mg of KBr. Infrared spectra were obtained using a PerkinElmer FTIR1650 spectrometer.

2.1.2.4. Humidity, apparent density and specific surface area. To determine the residual humidity of the biosorbent, a known amount of biomass was dried for 24 h at 105 °C in an oven. The biomass humidity (%) was calculated from the ratio of mass loss during drying to the initial biosorbent mass. The apparent density of the biomass ρ_{app} was determined by pycnometry. The effective surface area of the biosorbent was approximated as the external surface of biomass particles. Assuming that the biomass particles are spherical, their external surface per unit volume of test solution is

$$S = \frac{6m}{d_p \rho_{app} V_{sol}} \quad (3)$$

where m is the sorbent mass suspended in the test solution, d_p the mean diameter of sorbent particles, and V_{sol} the solution volume.

The specific surface area of the biomass S_p was calculated from the following expression:

$$S_p = \frac{6}{d_p \rho_{app}} \quad (4)$$

2.2. Biosorption tests

Calibrated solutions of potassium haxacyanoferrate in deionized water with varying concentrations were prepared. Batch biosorption tests were performed in duplicate at ambient temperature in 1-dm^3 flasks equipped with magnetic stirring. A known amount of *P. mutilus* biomass was added to 500 cm^3 of deionized water. The pH was adjusted to the desired level using 0.1N NaOH or 0.1N HCl. Then (at time 0 of the test) the fungal suspension was supplemented with a given volume of calibrated $K_3Fe(CN)_6$ solution to yield initial iron(III)–cyanide ion concentrations ranging between 0.1 and 3000 mg dm^{-3}. The residual concentration of complex ions at time t was determined iodometrically [23] after filtration of the sample through 8-μm-pore-size filter paper. The solid phase concentration of iron(III)–cyanide ions at time t (q_t) was calculated as follows:

$$q_t = \frac{C_0 - C_t}{X} \quad (5)$$

where C_0 and C_t are the concentrations of complex ions at time 0 and at time t, respectively, and X is the concentration of the biomass suspension ($X = m/V_{sol}$).

To build adsorption isotherms, varying C_0 concentrations were used and a single titration of hexacyanoferrate ions was performed after biosorption for 48 h, a period sufficient to reach equilibrium. The solid phase concentration of complex ions at equilibrium (q_e) was calculated from C_e, i.e., the C_t value at equilibrium:

$$q_e = \frac{C_0 - C_e}{X} \quad (6)$$

2.3. Theory

2.3.1. Adsorption kinetics

Two simplified kinetic equations are very frequently used to model the adsorption process for a wide range of solute–sorbent systems, including metal ions and natural biosorbents: the pseudo-first-order and pseudo-second-order equations proposed initially par Lagergren [24] and Ho and McKay [25], respectively:

2.3.1.1. Pseudo-first-order kinetic model (Lagergren's equation).

$$\frac{dq_t}{dt} = k_1(q_e - q_t) \quad (7)$$

where k_1 is the pseudo-first-order rate constant for the adsorption process.

After integration between $t = 0$ and $t = t$, Eq. (7) becomes:

$$\ln(q_e - q_t) = \ln(q_e) - k_1 t \quad (8)$$

The plot of $\ln(q_e - q_t)$ versus t gives a straight line for first-order kinetics. The value of k_1 is equal to the slope of this straight line.

2.3.1.2. Pseudo-second-order kinetic model (Ho's equation).

$$\frac{dq_t}{dt} = k_2(q_e - q_t)^2 \quad (9)$$

where k_2 is the rate constant of pseudo-second-order adsorption.

Integrating Eq. (9) between $t = 0$ and $t = t$ gives:

$$\frac{1}{q_e - q_t} = \frac{1}{q_e} + k_2 t \quad (10)$$

If the pseudo-second-order kinetic model is applicable, the plot of Eq. (10) gives a straight line whose slope is equal to k_2.

2.3.2. Diffusion models

Sorption kinetics are generally controlled by various factors including the following four steps: (i) solute transfer from the solution to the boundary film surrounding the particle (bulk diffusion), (ii) diffusion of the solute through the boundary layer to the surface of the sorbent (film diffusion), (iii) diffusion from the surface to intraparticle sites (intraparticle diffusion) and (iv) solute adsorption at active sites of the particle via mechanisms of ion exchange, precipitation, complexation and/or chelation. Processes (ii) and (iii) are likely to be rate controlling and various kinetic equations have been proposed to model these processes.

2.3.2.1. Film diffusion. During the first steps of adsorption, the intraparticle resistance is negligible and the transport is mainly due to film diffusion mechanism. The change in adsorbate concentration as a function of time can be written according to the film diffusion model proposed by Spahn and Schlünder [26]:

$$\frac{dC_t}{dt} = -k_L S(C_t - C_{st}) \quad (11)$$

where C_{st} is the surface concentration of adsorbate at time t, k_L is the external (liquid-film) mass transfer coefficient and S the specific surface area for mass transfer (i.e., the ratio of the sorbent exchange surface to the reactor volume).

Assuming that the surface concentration of adsorbate is negligible and $C_t = C_0$ during the initial stages of adsorption, Eq. (11) can be simplified as

$$\frac{d(C_t/C_0)}{dt} = -k_L S \quad (12)$$

Integrating Eq. (12) yields:

$$\ln\left(\frac{C_t}{C_0}\right) = -k_L S t \quad (13)$$

The value of k_L can be obtained from the slope of $\ln(C_t/C_0)$ as a function of time for the low t values.

2.3.2.2. Intraparticle diffusion. Various models have been reported to describe the intraparticle diffusion kinetics, in particular those proposed by Weber and Morris [27] and Urano and Tachikawa [28]:

- Weber and Morris model [27]:
  This model assumes the dependence of q_t (or C_t) on the square root of time:

$$C_0 - C_t = k_i t^{0.5} \quad (14)$$

  where k_i is the intraparticle diffusion coefficient.
- Urano and Tachikawa model [28]:
  The sorption kinetics is modelled by the following equation:

$$\ln\left[1 - \left(\frac{q_t}{q_e}\right)^2\right] = -\frac{4\pi^2 D_i}{d_p^2} t \quad (15)$$

  where q_t and q_e are solute concentrations in the solid (biomass) at t and at equilibrium, respectively, d_p is the mean particle diameter and D_i is the average diffusion coefficient in the solid.

The value of D_i can be determined from the slope of $\ln[1-(q_t/q_e)^2]$ as a function of time.

2.3.3. Sorption equilibrium

Adsorption isotherms describe the solute–sorbent interactions. Among a number of isotherm equations available for analyzing experimental sorption equilibrium data, the most applied are the Langmuir [29] and the Freundlich [30] models.

2.3.3.1. Langmuir isotherm. The Langmuir model assumes monolayer adsorption at specific homogeneous sites on the sorbent surface. Therefore, the sorbent has a finite capacity for the adsorbate (at equilibrium, a saturation point is reached beyond which no further adsorption can occur):

$$q_e = \frac{q_m b C_e}{1 + b C_e} \quad (16)$$

where q_e and C_e are the solute concentration in liquid (bulk solution) and solid (sorbent) phases at equilibrium, respectively, q_m is the maximum solid phase concentration of adsorbate (forming a complete monolayer coverage on the sorbent surface) and b is the Langmuir constant related to solute affinity for the sorbent-binding sites.

A linear form of (16) is

$$\frac{C_e}{q_e} = \frac{1}{q_m b} + \frac{C_e}{q_m} \quad (17)$$

The values of q_m and b can be obtained by plotting C_e/q_e against C_e.

Table 1
Acid–base potentiometric assessment of functional groups in various biomass types

Biomass type	pK_a	Groups	Ref.
Corynebacterium glutamicum Gram-positive soil bacterium	3.5–5.0 6.9 8–10	Carboxylic Phosphate Amine	[31]
Sphaerotilus natans Gram-negative wastewater bacterium	5 8.6	Carboxylic Phosphate	[32]
Spirulina sp. blue-green freshwater microalga (cyanobacterium)	2.1–3.1 6.8–7.8 10.8–11.7	Carboxylic Phosphate Hydroxyl, amine	[33]
Chaetophora elegans green freshwater alga	6.6–7.3 8.2–10.5	Carboxylic Amine, phenol	[34]
Sargassum wightii marine brown alga	4.3 8.8	Carboxylic Amine	[35]

2.3.3.2. Freundlich isotherm. The Freundlich isotherm is an empirical model that applies to adsorption on heterogeneous surfaces and is expressed by the following equation:

$$q_e = K_F C_e^{1/n} \quad (18)$$

with its logarithmic form:

$$\ln(q_e) = \ln(K_F) + \frac{1}{n}\ln(C_e) \quad (19)$$

where C_e is the equilibrium concentration of the adsorbate in bulk solution and K_F and n are Freundlich constants. The K_F constant is an indicator of the adsorption capacity of the sorbent while $1/n$ reflects the adsorption intensity.

The plot of $\ln(q_e)$ versus $\ln(C_e)$ allows the determination of the Freundlich constants.

3. Results and discussion

3.1. Biomass characterization

3.1.1. Potentiometric titration and overall biomass charge

P. mutilus biomass contains polysaccharides, proteins and lipids and can be considered as a polyelectrolyte with amino, carboxyl, phosphate and sulfate groups. The acid–base potentiometric titration allows identifying those ionisable functional groups or binding sites that can act as ligands in biosorption phenomena. This method was used successfully in several works on various biomass types (Table 1).

The titration curves of the raw and pre-treated biomasses (Fig. 1) show the existence of several inflection points which correspond to

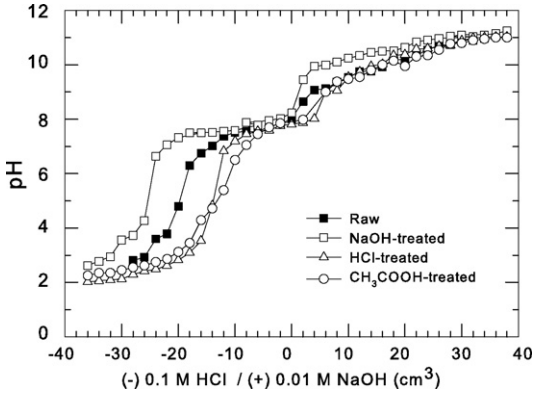

Fig. 1. Acid–base potentiometric titration of crude or pre-treated *Pleurotus mutilus* biomass. Particles with diameters ranging from 50 to 80 μm were used.

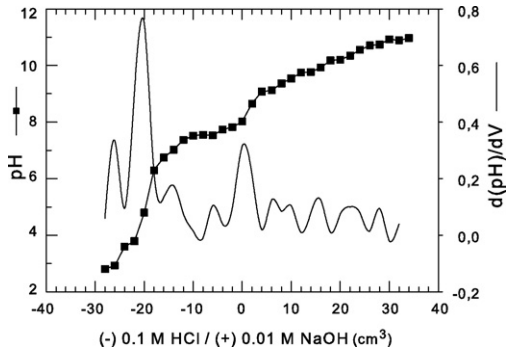

Fig. 2. Determination of acid functions of the biomass using the second derivative curve of pH vs. titrant volume: example of crude biomass.

the end points and consequently provide the equivalence volumes and the values of pK_a for the prevalent functional groups on the biosorbent surface. A precise evaluation of these inflection points is difficult but is somewhat facilitated by searching for zero values of the second derivative of pH versus titrant volume, which correspond to maximum and minimum values of the first derivative (Fig. 2). According to this graphical determination, three main inflection points could be distinguished on the titration curves, corresponding to ionization of the major functional groups participating in ion binding. The first one was located between pH 4.8 and pH 5.4 and corresponded to carboxylic groups whose pK_a values range between 2 and 5 depending on the aliphatic or aromatic character of the carboxylic function [36]. The second inflection point, between pH 8.6 and pH 9.4, was that of phosphate groups. The last one, at pH 9.1–10.6, represented the amino groups of protein materials and the phenolic groups of acids [37].

Fig. 3 shows the pH-dependence of biomass overall charge calculated using Eqs. (3) and (4). A logical decrease in the overall charge of the four tested biomass samples was observed as pH increased. At acidic pH, the positive overall charge of the biosorbent was due primarily to the protonation of amino groups provided by proteins, the carboxylic groups being neutral or partially negative. As pH increased, protonated amino groups were progressively neutralized; conversely carboxylic (and phosphate groups) became negatively charged. The overall absolute charge of the untreated biomass at pH 3 was three times higher than at pH 12. This indicates that the quantity of amino groups in the biomass was high compared to carboxylic ones.

The zeta potential of biomass particles was also a decreasing function of pH in the pH 3–8 range (Fig. 4). Zeta potential is the electrical potential at the surface of a particle. It characterizes the charge of a particle with a bound layer of counterions attached to its surface. The zeta potential of a number of biosorbent particles, including bacteria [38], cyanobacteria [39], yeasts [40], fungi [41], lichens [42], aquatic [43] and terrestrial [44] plant materials, has been shown to be a decreasing function of pH.

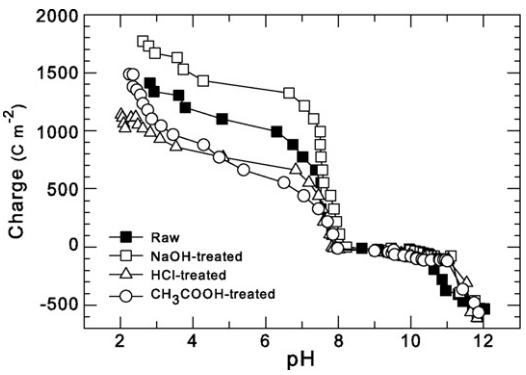

Fig. 3. Evolution of the overall electrical charge of the biomass as a function of initial pH of the liquid medium (50–80-μm diameter particles).

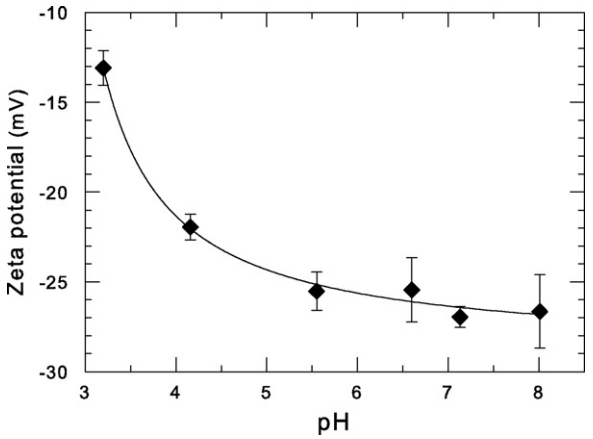

Fig. 4. Zeta potential of crude biomass particles as a function of initial pH of the liquid medium (50–80-μm diameter particles).

3.1.2. Infrared spectroscopy

Infrared analysis allows identification of some characteristic peaks from functional groups, including those implied in biosorption. The complex IR spectra of native, acid and alkali-treated *P. mutilus* biomass fractions (Fig. 5) confirmed the presence of R–NH_2 amino groups (amino acids, proteins, glycoproteins, etc.), carboxylic acids (fatty acids, lipopolysaccharides, etc.), sulfonates and phosphates (Table 2).

The different chemical treatments induced no significant shifts or changes in intensity of the characteristic absorbance bands, with only slight peak shifts and/or intensity changes at 1642 cm^{-1} and for bands <800 cm^{-1}, the disappearance of peaks at 1740 and 1410 cm^{-1} for acid-treated biomass, and the disappearance of weak peak at 1230 cm^{-1} for acid- or alkali-treated biomass. It is difficult to propose a precise interpretation of these minor modifications that probably involved carboxylic groups (Table 2) whose protonation/esterification levels were modified by pre-treatment.

3.2. Biosorption tests

3.2.1. Determination of optimal operating conditions for biosorption

To optimize the biosorption efficiency of *P. mutilus* biomass, biosorption experiments were first performed under varying operating conditions relating to the biosorbent (biomass chemical pre-treatment, concentration and particle size), the sorbate (hexacyanoferrate concentration) and the test medium (initial pH, agitation speed).

3.2.1.1. Effect of initial pH and biomass pre-treatment. Fig. 6 shows the biosorption kinetics of hexacyanoferrate ions by crude *P. mutilus* biomass at low and high initial pH of the liquid medium. At both pHs, the uptake of complex ion by the fungal biomass was slow in comparison with most reported data on (free) metal ion adsorption by various biosorbents: a minimum contact time of about 24 h was necessary to achieve the sorption equilibrium. In contradiction with the pH-charge profile of the biomass, the biosorption capacity was noticeably lower at acid pH than at high pH. The biosorption efficiency of all biomass fractions, crude or pre-treated, was low at acidic or neutral pH and increased rapidly at pH higher than

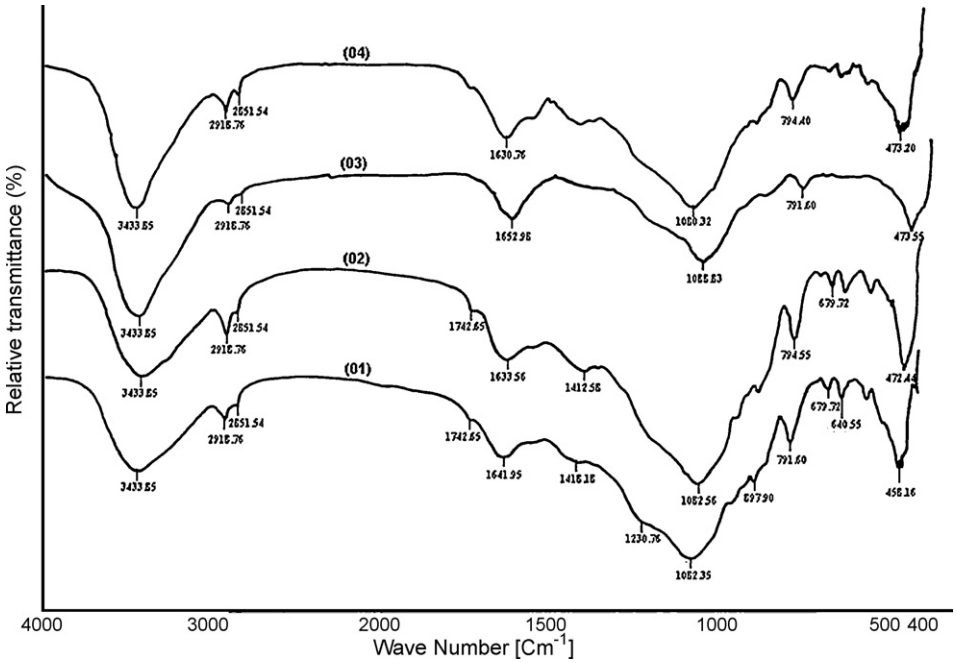

Fig. 5. Infrared spectra of crude or pre-treated biomass (50–80-μm diameter particles). (1) Crude, (2) NaOH-treated, (3) HCl-treated and (4) CH_3COOH-treated biomass.

11 (Fig. 7). A very similar effect of initial pH on the biosorbent efficiency at equilibrium has been reported by Aksu et al. using *Rhizopus arrhizus* biomass for iron(III)–cyanide ion biosorption [21]. No convincing explanation of this behaviour was given by these authors, however.

Various mechanisms have been proposed to try to explain the adsorption of a negative complex on a negatively charged surface, in particular as concerns the adsorption of gold and silver cyanide on activated carbon in the weakly acidic and alkaline pH ranges. Since electrostatic adsorption of complex ions is excluded, adsorption may proceed by way of chemisorptive interactions, possibly at uncharged active centres [45]. Adsorption involving ion pairs, whose formation leads to charge neutralization of the adsorbing species, and adsorption of unpaired ions implying strong adsorbate–adsorbent interactions that exceed the electrostatic repulsion, are the two most widely accepted theories (see Ref. [46] and references therein).

These results show that the elimination of the cyanide complex is effective in alkaline medium only. After alkalinization, effluents bearing cyanide and metal ions like those produced by mining or surface treatment industries will contain free or metal-combined cyanides in addition to trace metal ions—since most metal ions, including ferric or ferrous iron, will be precipitated as hydroxides due to their low solubility constants. The treatment of these industrial effluents by biosorption on *P. mutilus* may be advantageous knowing that the cyanide ion is very unstable and volatile in acid medium.

At pH 12.5, the crude and CH_3COOH-treated biomass particles showed very similar biosorption efficiencies, noticeably higher than those obtained for NaOH- and HCl-treated ones. However, the positive/negative influence of acid/base pre-treatment on biosorption capacity was low compared to that reported by others [47].

Table 2
IR absorption bands and corresponding possible groups

Wave number (cm^{-1})	Band intensity[a]	Assignment	
		Functional groups	Bonds
3434	S (broad)	Amide, amine Alcohol	N—H stretching O—H stretching
2919	S (narrow)	Carboxylic acid Alkane	O—H stretching C—H stretching
1743	W	Carboxylic acid, ester	C=O stretching
1642	A	Amide Amine Alkene	C=O stretching N—H bending C=C stretching
1418	A	Sulfate Alkane Phenol Carboxylic acid	S=O stretching C—H bending O—H stretching C=O stretching
1231	W	Carboxylic acid, ester, anhydride	C—O stretching
1082	S (broad)	Ether, alcohol, ester	C—O stretching
898	A	Alkene	C—H bending
<800	A	Phosphate, sulfonate, sulfide	

[a] S: strong; A: average; W: weak.

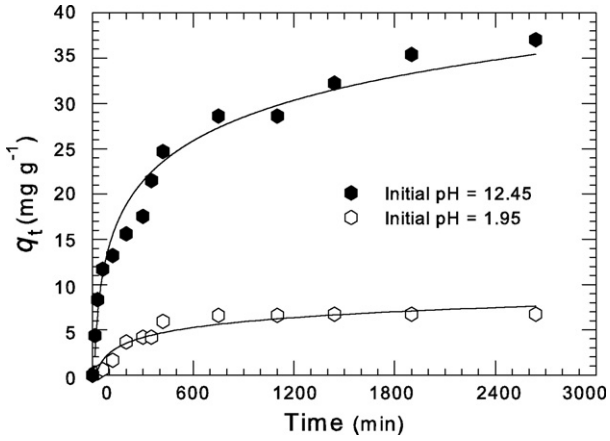

Fig. 6. Biosorption kinetics of hexacyanoferrate anions by crude *P. mutilus* biomass particles (50–80-μm diameter) at acid and alkaline pHs (hexacyanoferrate concentration, 150 mg dm^{-3}; biomass concentration, 3.0 g dm^{-3}; stirring speed, 150 rpm).

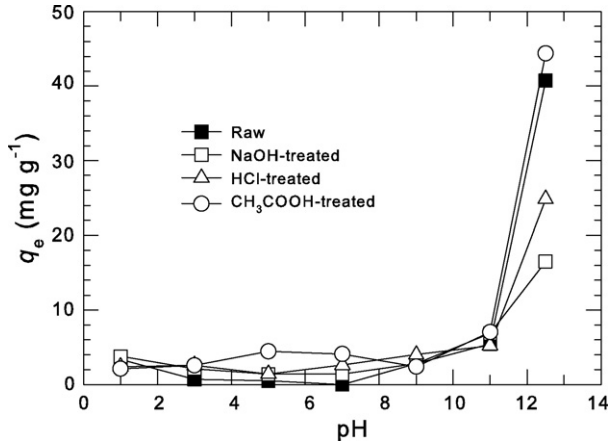

Fig. 7. Adsorption capacity of *P. mutilus* biomass (50–80-μm diameter particles) as a function of initial pH of the liquid medium (hexacyanoferrate concentration, 150 mg dm^{-3}; biomass concentration, 3.0 g dm^{-3}; stirring speed, 150 rpm).

As a consequence, a highly alkaline initial pH of 12.5 was selected for the next biosorption tests that were performed using crude biomass.

3.2.1.2. Effects of biomass and hexacyanoferrate concentrations. In the range of the tested complex ion concentrations (100–1000 mg dm^{-3}), the equilibrium capacity of *P. mutilus* biomass reached a maximum value for an initial biosorbent concentration of *ca.* 0.3 g dm^{-3} (Fig. 8). On the other hand, the absolute amount of complex ion adsorbed increased with the biosorbent concentration owing to an increasing adsorption surface area (not shown). The decrease in q_e value as biomass concentration increases is a frequently reported observation [21,31,38,40] and may be due to partial particle aggregation causing a decrease in specific surface area of the biosorbent.

At a given initial concentration of biomass, in particular at the optimal concentration of 0.3 g dm^{-3}, the q_e value was an increasing function of the initial concentration of complex ions (Fig. 8). However, the percentage of adsorbed hexacyanoferrate was noticeably higher at moderate C_0 value, reaching *ca.* 24% at C_0 = 150 mg dm^{-3} compared to 7% at C_0 = 975 mg dm^{-3}. Therefore, initial concentrations of 0.3 g dm^{-3} biomass and 150 mg dm^{-3} hexacyanoferrate were chosen for next experiments.

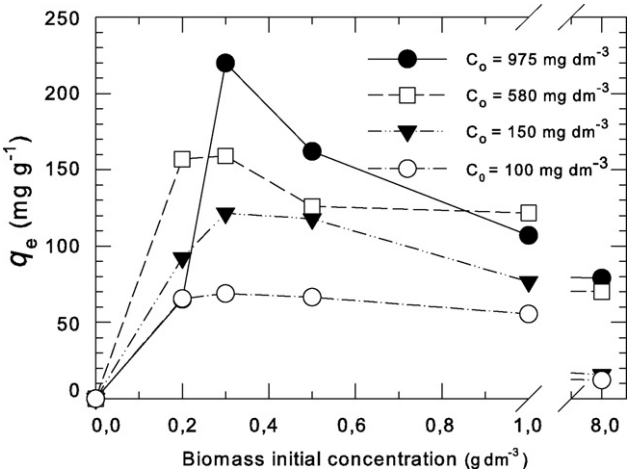

Fig. 8. Influence of biomass concentration (crude biomass; 50–80-μm diameter particles) on adsorption efficiency for different initial concentrations of hexacyanoferrate ions (initial pH, 12.5; stirring speed, 250 rpm).

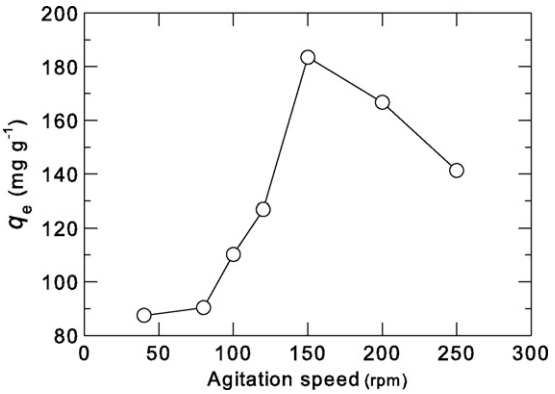

Fig. 9. Influence of stirring speed on adsorption efficiency (crude biomass; 50–80-μm diameter particles; initial pH, 12.5; hexacyanoferrate concentration, 150 mg dm^{-3}; biomass concentration, 0.3 g dm^{-3}).

3.2.1.3. Effect of stirring speed. The biosorption efficiency of the biomass was noticeably affected by the stirring speed of the particle suspension (Fig. 9). The q_e value increased with the agitation speed to reach a maximum at 150 rpm. A higher probability of collision between adsorbing ions and biosorbent particles, together with a decrease in external mass transfer resistance (i.e., increased bulk and film diffusion of complex ions) explain this effect as a consequence of turbulence enhancement. The biosorption capacity decreased at higher agitation speed that affected the homogeneity of the biomass particle suspension due to vortex formation. A stirring speed of 150 rpm was selected from these results.

3.2.1.4. Effect of biomass particle size. Fig. 10 shows the influence of the mean diameter of biomass particles (d_p) on the biosorbent ability to adsorb complex ions. The q_e value was an increasing function of d_p, reaching a maximum for the 315–400-μm fraction and stabilizing at higher d_p value. This evolution was observed for the crude biomass and all other biomass types, acid- or alkali-treated, the crude and CH_3COOH-treated particles remaining the most efficient for all tested sizes. It contradicts most published data that underline the favourable effect of a decrease in biosorbent particle size on biosorption efficiency—the smaller the particle, the larger its specific area (S_p). Probably the benefit of a higher available interfacial area was offset by enlarged intraparticular diffusion resistance for the smaller *P. mutilus* particles.

From these preliminary results, the following conditions were used for kinetic and equilibrium biosorption experiments: crude and CH_3COOH-pre-treated biomass; initial pH, 12.5; biosorbent

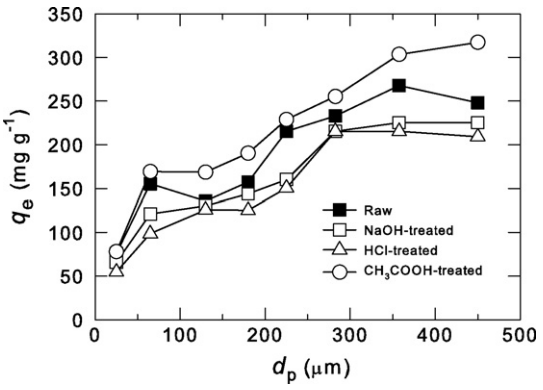

Fig. 10. Influence of particle size on adsorption efficiency of crude and pre-treated biomass granules (initial pH, 12.5; hexacyanoferrate concentration, 150 mg dm^{-3}; biomass concentration, 0.3 g dm^{-3}).

Table 3
Physical characteristics of the biomass

Biomass type	Particle size, d_p (μm)	Humidity (%)	Apparent density, ρ_{app} (g cm^{-3})	Specific area[a], S_p (m^2 g^{-1})
Crude	50–80	3.70	0.66	0.14
CH_3COOH-treated	50–80	1.81	0.60	0.15
Crude	315–400	2.50	0.52	0.03
CH_3COOH-treated	315–400	2.60	0.55	0.03

[a] An average value of d_p was used for calculations.

concentration, 0.3 g dm^{-3}; initial hexacyanoferrate concentration, 150 mg dm^{-3} (kinetic experiments); agitation speed, 150 rpm. In addition, two biomass particle sizes were tested, i.e., the finest particles resulting from biomass grinding (50–80 μm) and the largest ones leading to optimal sorption efficiency (315–400 μm). Some physical characteristics of the selected two biomass fractions are given in Table 3.

3.2.2. Kinetic experiments and modelling

The biosorption kinetics of hexacyanoferrate ions by *P. mutilus* biomass particles in the optimal operating conditions defined above are shown in Fig. 11. In such optimized conditions, these kinetics remained slow: about 5 h of contact were necessary to reach 50% of the maximum (equilibrium) sorption capacity (q_e) which, at the tested initial concentration of complex ions (i.e., 150 mg dm^{-3}), amounted to 185 and 310 mg g^{-1} for crude biomass particles with 50–80 and 315–400 μm diameters, respectively. The q_e values for CH_3COOH-treated biomass particles were slightly higher, i.e., 205 and 335 mg g^{-1}. To clarify the mechanisms controlling the adsorption process, these experimental data were compared to some standard kinetic models.

3.2.2.1. Pseudo-first-order and pseudo-second-order models. The values of the rate constants for the pseudo-first-order (k_1) and pseudo-second-order (k_2) sorption reaction were obtained respectively by plotting the linearity of $\ln(q_e - q_t)$ versus t (Eq. (8)) and of $1/(q_e - q_t)$ versus t (Eq. (10)). The rate constants for kinetic modelling of complex ions uptake are presented in Table 4. The experimental adsorption kinetics were adequately described by both Lagergren and Ho relationships, with correlation coefficients close to 1, Eq. (10) giving slightly better fits for the 50–80 μm particles. The rate constants k_1 and k_2 decreased as the particle size increased and as a consequence of biomass pre-treatment with acetic acid.

Table 4
Rate constants of pseudo-first-order and pseudo-second-order diffusion models

Biomass type	Pseudo-first-order		Pseudo-second-order	
	k_1 ($\times 10^3$ min^{-1})	R^2	k_2 ($\times 10^5$ g mg^{-1} min^{-1})	R^2
Raw, 50–80 μm	2.66	0.957	2.51	0.985
Treated, 50–80 μm	2.57	0.959	1.58	0.993
Raw, 315–400 μm	1.24	0.983	1.21	0.977
Treated, 315–400 μm	0.79	0.990	0.41	0.995

The pseudo-first-order and pseudo-second-order models assume that the biosorption rate is proportional to the number (or the square of number) of unoccupied sites at the biosorbent surface. An increase in rate constants with decreasing particle size has been frequently observed and attributed to the larger total surface area of small particles [48]. According to these models, biomass pre-treatment reduced the number of free sites at the particle surface: since the best biosorption efficiency was obtained for large, pre-treated biomass granules, biosorption of hexacyanoferrate ions by *P. mutilus* biomass was very probably not limited to the particle surface.

3.2.2.2. External mass transfer (film diffusion) model. The initial external diffusion rate ($k_L A$ in Eq. (13)) and the corresponding (liquid-film) mass transfer coefficient k_L, obtained from the slope of $\ln(C_t/C_0)$ as a function of time for the low t values (Fig. 12), were increased by increasing the biomass particle size (Table 5). Therefore, the use of large particles favoured external mass transfer. The k_L values were low compared to reported data on various metal ion-biosorbent systems, including free metal ions V(IV) and chitosan [49], complex, negatively charged Cr(VI) ions and chitin [50], or else Cu(II) ions and waste sugar beet pulp [51].

3.2.2.3. Intraparticle diffusion models. In agreement with a number of published data [52–54], intraparticle diffusion plots according to the Weber and Morris model (Eq. (14)) presented two successive linear regions, the first straight line showing a steeper slope than the second one (Fig. 13). These linear relationships between the sorption efficiency of biomass particles and the root of contact time indicate that the rate-controlling step of complex ion biosorption was essentially intraparticle diffusion. The bi-linearity of the plots may be attributed to the existence of two different classes of pores in the biosorbent structure, i.e., macropores and micropores.

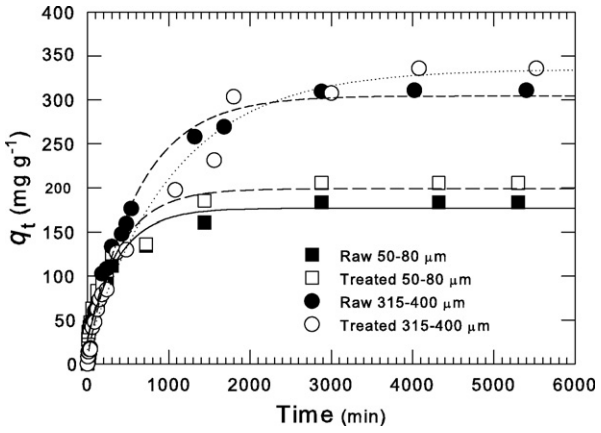

Fig. 11. Adsorption kinetics of hexacyanoferrate anions by biomass particles with optimized operating conditions (initial pH, 12.5; hexacyanoferrate concentration, 150 mg dm^{-3}; biomass concentration, 0.3 g dm^{-3}; agitation speed, 150 rpm) and use of crude and CH_3COOH-treated biomass granules with 50–80 μm or 315–400 μm diameter.

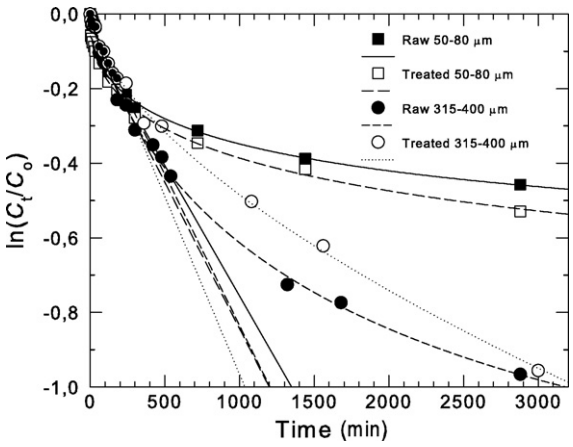

Fig. 12. Plots of $\ln(C_t/C_0)$ vs. time for determination of the mass transfer coefficient of complex ions through the stagnant film surrounding biomass particles (external diffusion).

Table 5
External and intraparticle diffusion coefficients

Biomass type (R, raw; T, treated)	Initial liquid-film mass transfer coefficient[a]			Intraparticle diffusion rate constant[b]			Average diffusion coefficient[b]	
	k_LS ($\times10^5$ s^{-1})	k_L ($\times10^7$ m s^{-1})	R^2	k_{i1}[c]	k_{i2}[c]	R^2	D_i ($\times10^{15}$ m^2 s^{-1})	R^2
R, 50–80 μm	1.16	2.8	0.917	0.75		0.986	1.8	0.989
					0.22	0.917		
T, 50–80 μm	1.31	2.9	0.924	0.71		0.964	1.5	0.971
					0.24	0.944		
R, 315–400 μm	1.35	15.0	0.960	1.03		0.984	46.0	0.992
					0.27	0.907		
T, 315–400 μm	1.59	17.6	0.977	0.76		0.992	22.2	0.996
					0.18	0.716		

[a] External diffusion.
[b] Intraparticle diffusion.
[c] k_i (mg g^{-1} s$^{-0.5}$).

The values of the corresponding intraparticle diffusion rate constants k_{i1} and k_{i2} (Table 5) were in the range of [53,55] or, more frequently, superior to [52,54,56–58] those given by others for a variety of sorbent–sorbate couples. The rate constants k_{i1} and k_{i2} characterizing diffusion of complex ions in 315–400 μm diameter particles were somewhat higher than those determined for smaller granules. In addition, biosorption rate control by micropore diffusion occurred more rapidly in 50–80 μm biomass particles than in larger ones. This may indicate reduced accessibility of adsorbing ions to the macroporous volume of the biosorbent and/or some clogging of macropores in thin particles. The process of complex ion biosorption by thin biomass particles began with macropore diffusion whereas the Weber and Morris plots displayed a nonlinear portion during the early contact times for 315–400 μm biosorbent particles, indicating that biosorption by larger particles was also affected by boundary film diffusion during this period.

A fairly linear distribution of experimental biosorption data was also obtained by applying the Urano and Tachikawa model (Eq. (15), Fig. 14). The D_i values were significantly higher for large biomass particles than for thinner ones, but remained very low compared to the diffusion coefficient of hexacyanoferrate ions in water, i.e., around 7×10^{-10} m^2 s^{-1} [59,60]. They were in the range of literature data [49,54,56], however.

3.2.3. Equilibrium experiments and modelling

The effect of the initial concentration of iron(III)–cyanide ions on the biosorption efficiency of crude and pre-treated biomass particles is shown in Fig. 15. Whatever the particle size, the maximum capacity for the two types of biomass was reached for an initial concentration of complex ions around 1200 mg dm^{-3}. The highest q_e value, namely 616 mg g^{-1}, was displayed by granules of CH_3COOH-treated biomass with diameters in the 315–400 μm range.

From linearized Langmuir (Eqs. (16) and (17)) and Freundlich (Eqs. (18) and (19)) isotherms of complex ions, Langmuir and Freundlich parameters characterizing adsorption capacity (q_m, K_F) and affinity (b, n) of *P. mutilus* particles for complex ions and their correlation coefficients (R^2) were calculated (Table 6). Both models satisfactorily fitted the biosorption equilibrium data, indicating a monolayer sorption mechanism. Better correlation coefficients were obtained for the Langmuir equation, however.

The results obtained for the most efficient biomass particles (pre-treatment with acetic acid, 315–400 μm diameter) are very

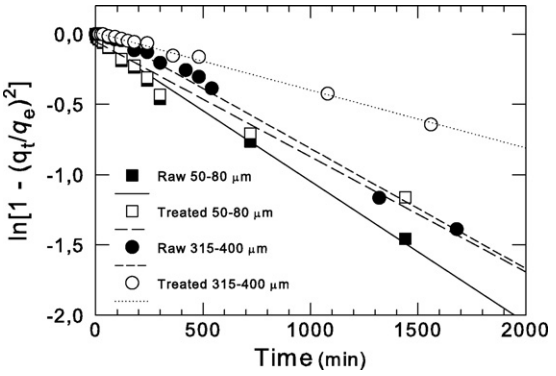

Fig. 14. Intraparticle diffusion plots according to Urano and Tachikawa model.

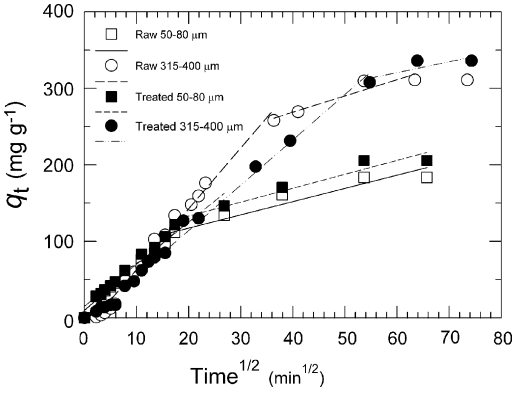

Fig. 13. Intraparticle diffusion kinetics for complex ion biosorption on crude and pre-treated biomass particles according to the Weber and Morris model.

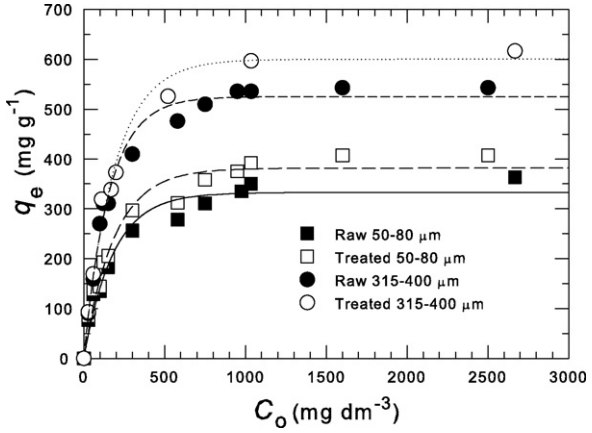

Fig. 15. Effect of varying initial concentrations of hexacyanoferrate ions on the biosorption efficiency of *P. mutilus* biomass (initial pH, 12.5; biomass concentration, 0.3 g dm^{-3}; agitation speed, 150 rpm). Crude and CH_3COOH-treated biomass granules with 50–80 μm or 315–400 μm diameter were used.

Table 6
Sorption isotherm coefficients of Langmuir and Freundlich models

Biomass type	Langmuir			Freundlich		
	q_m (mg g^{-1})	b (dm^3 mg^{-1})	R^2	K_F (mg$^{(n-1)/n}$ dm$^{3/n}$ g^{-1})	n	R^2
Raw, 50–80 μm	373.2	0.0113	0.997	54.1	3.79	0.966
Treated, 50–80 μm	420.0	0.0125	0.997	66.0	3.97	0.964
Raw, 315–400 μm	550.8	0.0308	0.999	115.5	4.41	0.928
Treated, 315–400 μm	623.8	0.0282	0.999	178.6	6.11	0.932

similar to those reported by Aksu et al. [21] for biosorption of iron(III)–cyanide ions to *R. arrhizus* biomass at pH 13.

4. Conclusion

In this study, adsorption of iron(III)–cyanide on *P. mutilus* fungal biomass in crude or acid/alkali-treated form has been monitored in batch assays. Biosorption efficiency was shown to be affected by various experimental parameters including biomass pre-treatment, particle size and initial pH of the complex ion solution.

Adsorption capacity was little modified by acid/alkali treatments compared to native biomass, avoiding the need for time consuming and costly pre-treatment stages of the biosorbent. The maximum efficiency of crude and pre-treated biomass was reached for particle size between 315 and 400 μm. This particle size is higher than those commonly tested in batch biosorption experiments, e.g., metal biosorption with powdered bacterial [48], fungal [61,62] or algal biomass [63], but somewhat lower than those recommended by Volesky [19] for continuous experiments. It may be therefore a good compromise between maximum mass transfer into the particles and minimum resistance to liquid flow in continuous (columnar) processes [19].

Although *P. mutilus* cell wall contained chemical groups conferring to this biomass an overall positive charge in acid medium (amine groups) and a negative charge in basic conditions (carboxylic, phosphate groups), the best performance of the complex anion biosorption was obtained at strongly alkaline pH, i.e., around 12. Therefore, under the conditions of optimal pH, this biosorbent can be used successfully in operating conditions that allow the simultaneous removal of complex metal–cyanide ions (by adsorption) and free metal ions (by precipitation) likely to coexist in industrial wastewaters with no possibility of free cyanide liberation as HCN.

The adsorption kinetics of iron(III)–cyanide ions on *P. mutilus* particles was also discussed in the light of classical models for surface adsorption, film diffusion and intraparticle mass transfer. Both surface adsorption and intraparticle diffusion contributed to the actual adsorption process. The equilibrium adsorption data fitted well to the Freundlich and Langmuir isotherm models. The maximum monolayer capacity of fungal biomass in optimal operating conditions was over 600 mg g^{-1}, in the range of the values reported by others [21].

In conclusion, this study demonstrates that the dried *P. mutilus* biomass may be used as an effective biosorbent for the treatment of wastewater containing complex cyanided ions. *P. mutilus* is not only an abundant industrial waste and may be an alternative to more costly materials, such as the widely used activated charcoal but also microbial biomass specifically cultivated for the sole purpose of biosorption. However, the relatively slow biosorption kinetics of the complex anion, controlled primarily by intraparticle diffusion, is a negative feature for practical development of this material. These preliminary batch experiments must therefore be followed by additional tests in a continuous system (column reactor) with improved adsorption/desorption rates to confirm the technical and economic interests of this biosorbent. Such tests are being performed and results will be published in the near future.

Acknowledgements

The authors would like to acknowledge the Ministry of Higher Education and Scientific Research of Algeria for their financial support provided by the Exceptional National Program (PNE) for postgraduate students. We would like also to greatly thank all the team members of the Laboratory LEDTEDGE of the Ecole Normale Supérieure of Kouba in Algiers and the Laboratory of Polymers, Biopolymers and Surfaces (PBS) of the University of Rouen in France for their cooperation and fruitful advices.

References

[1] D.B. Donato, O. Nichols, H. Possingham, M. Moore, P.F. Ricci, B.N. Noller, A critical review of the effects of gold cyanide-bearing tailings solutions on wildlife, Environ. Int. 33 (2007) 974–984.
[2] R. Eisler, Cyanide hazards to fish, wildlife, and invertebrates: a synoptic review, U.S. Fish Wildl. Serv., Biol. Rep. 85 (1.23) (1991).
[3] L.E Towill, J.S. Drury, B.L. Whitfield, E.B. Lewis, E.L. Galyan, A.S. Hammons, Reviews of the environmental effects of pollutants. V. Cyanides, Interagency Rept. Oak Ridge Natl. Lab. Rept. No. ORNL/EIS-81 and US EPA Rept. No. EPA-600/1-78-027, 1978.
[4] S.A.K. Palmer, M.A. Breton, T.J. Nunno, D.M. Sullivan, N.F. Surprenant, Technical Resource Document: Treatment Technologies for Metal/Cyanide-Containing Wastes, Volume III, US EPA Rept. No. EPA-60O/S2-87/106, 1988.
[5] M.M. Botz, Overview of cyanide treatment methods, in: Mining Environmental Management, Mining Journal Ltd., London, UK, 2001, pp. 28–30.
[6] A. Akcil, Destruction of cyanide in gold mill effluents: biological versus chemical treatments, Biotechnol. Adv. 21 (2003) 501–511.
[7] S. Ebbs, Biological degradation of cyanide compounds, Curr. Opin. Biotechnol. 15 (2004) 231–236.
[8] M.D. Adjei, Y. Ohta, Factors affecting the biodegradation of cyanide by *Burkholderia cepacia* strain C-3, J. Biosci. Bioeng. 89 (2000) (2000) 274–277.
[9] A.Y. Dursun, A. Calik, Z. Aksu, Degradation of ferrous(II) cyanide complex ions by *Pseudomonas fluorescens*, Process Biochem. 34 (1999) 901–908.
[10] C.M. Kao, C.C. Lin, J.K. Liu, Y.L. Chen, L.T. Wu, S.C. Chen, Biodegradation of the metal–cyano complex tetracyanonickelate(II) by *Klebsiella oxytoca*, Enzyme Microb. Technol. 35 (2004) 405–410.
[11] A. Dumestre, N. Bousserrhine, J. Berthelin, Biodegradation of free cyanide by the fungi *Fusarium solani*: relation to pH and cyanide speciation in solution, C. R. Acad. Sci. Paris Ser. IIA 325 (1997) 133–138.
[12] M. Barclay, V.A. Tett, C.J. Knowles:, Metabolism and enzymology of cyanide/metallocyanide biodegradation by *Fusarium solani* under neutral and acidic conditions, Enzyme Microb. Technol. 23 (1998) 321–330.
[13] M.I. Ezzi, J.M. Lynch, Biodegradation of cyanide by *Trichoderma* spp. and *Fusarium* spp., Enzyme Microb. Technol. 36 (2005) 849–854.
[14] F. Gurbuz, H. Ciftci, A. Akcil, A.G. Karahan, Microbial detoxification of cyanide solutions: a new biotechnological approach using algae, Hydrometallurgy 72 (2004) 167–176.
[15] X.Z. Yu, J.D. Gu, Effects of available nitrogen on the uptake and assimilation of ferrocyanide and ferricyanide complexes in weeping willows, J. Hazard. Mater. 156 (2008) 300–307.
[16] M. Larsen, S. Trapp, A. Pirandello, Removal of cyanide by woody plants, Chemosphere 54 (2004) 325–333.
[17] B. Volesky, Biosorbents for metal recovery, Trends Biotechnol. 5 (1987) 96–101.
[18] F. Veglio', F. Beolchini, Removal of metals by biosorption: a review, Hydrometallurgy 44 (1997) 301–316.
[19] B. Volesky, Detoxification of metal-bearing effluents: biosorption for the next century, Hydrometallurgy 59 (2001) 203–216.
[20] S.S. Ahluwalia, D. Goyal, Microbial and plant derived biomass for removal of heavy metals from wastewater, Bioresour. Technol. 98 (2007) 2243–2257.

[21] Z. Aksu, A. Calik, A.Y. Dursun, Z. Demircan, Biosorption of iron(III)–cyanide complex anions to *Rhizopus arrhizus*: application of adsorption isotherms, Process Biochem. 34 (1999) 483–491.
[22] Z. Aksu, H. Gulen, Binary biosorption of iron(III) and iron(III)–cyanide complex ions on *Rhizopus arrhizus*: modelling of synergistic interaction, Process Biochem. 38 (2002) 161–173.
[23] A. Vogel, A Textbook of Quantitative Inorganic Analysis, Theory and Practice, 9th ed., Lowe and Brydone, London, UK, 1948.
[24] Y.S. Ho, Citation review of Lagergren kinetic rate equation on adsorption reactions, Scientometrics 59 (2004) 171–177.
[25] Y.S. Ho, G. McKay, The kinetics of sorption of divalent metal ions onto sphagnum moss peat, Water Res. 34 (2000) 735–742.
[26] H. Spahn, U. Schlünder, The scale-up of activated carbon columns for water purification based on results from batch test. I. Theoretical and experimental determination of adsorption rates of single organic solutes in batch tests, Chem. Eng. Sci. 30 (1975) 529–537.
[27] W.J. Weber Jr., J.C. Morris, Kinetics of adsorption on carbon from solution, J. Sanit. Eng. Div. 89 (1963) 31–60.
[28] K. Urano, H. Tachikawa, Process development for removal and recovery of phosphorus from wastewater by a new adsorbent. 2. Adsorption rates and breakthrough curves, Ind. Eng. Chem. Res. 30 (1991) 1897–1899.
[29] I. Langmuir, The constitution and fundamental properties of solids and liquids. Part I. Solids, J. Am. Chem. Soc. 38 (1916) 2221–2295.
[30] H.M.F. Freundlich, Über die Adsorption in Lösungen (Over the adsorption in solution), Z. Phys. Chem. 57 (1906) 385–470.
[31] S.W. Won, S.B. Choi, Y.-S. Yun, Interaction between protonated waste biomass of *Corynebacterium glutamicum* and anionic dye Reactive Red 4, Colloid Surf. A 262 (2005) 175–180.
[32] A. Esposito, F. Pagnanelli, A. Lodi, C. Solicio, F. Veglio, Biosorption of heavy metals by *Sphaerotilus natans*: an equilibrium study at different pH and biomass concentrations, Hydrometallurgy 60 (2001) 129–141.
[33] K. Chojnacka, A. Chojnacki, H. Gorecka, Biosorption of Cr^{3+}, Cd^{2+} and Cu^{2+} ions by blue-green algae *Spirulina* sp.: kinetics, equilibrium and the mechanism of the process, Chemosphere 59 (2005) 75–84.
[34] A.D. Andrade, M.C.E. Rollemberg, J.A. Nobrega, Proton and metal binding capacity of the green freshwater alga *Chaetophora elegans*, Process Biochem. 40 (2005) 1931–1936.
[35] K. Vijayaraghavan, K. Palanivelu, M. Velan, Treatment of nickel containing electroplating effluents with *Sargassum wightii* biomass, Process Biochem. 41 (2006) 853–859.
[36] G. Naja, C. Mustin, B. Volesky, J. Berthelin, A high-resolution titrator: a new approach to studying binding sites of microbial biosorbents, Water Res. 39 (2005) 579–588.
[37] Z. Qiang, C. Adams, Potentiometric determination of acid dissociation constants (pK_a) for human and veterinary antibiotics, Water Res. 38 (2004) 2874–2890.
[38] M.X. Loukidou, A.I. Zouboulis, T.D. Karapantsios, K.A. Matis, Equilibrium and kinetic modeling of chromium(VI) biosorption by *Aeromonas caviae*, Colloid Surf. A 242 (2004) 93–104.
[39] M. Dittrich, S. Sibler, Cell surface groups of two picocyanobacteria strains studied by zeta potential investigations, potentiometric titration, and infrared spectroscopy, J. Colloid Interf. Sci. 286 (2005) 487–495.
[40] A. Bingol, H. Ucun, Y. Kemal Bayhan, A. Karagunduz, A. Cakici, B. Keskinler, Removal of chromate anions from aqueous stream by a cationic surfactant-modified yeast, Bioresour. Technol. 94 (2004) 245–249.
[41] D. Pokhrel, T. Viraraghavan, Arsenic removal from an aqueous solution by a modified fungal biomass, Water Res. 40 (2006) 549–552.
[42] F. Ekmekyapar, A. Aslan, Y.K. Bayhan, A. Cakici, Biosorption of copper(II) by nonliving lichen biomass of *Cladonia rangiformis* hoffm., J. Hazard. Mater. 137 (2006) 293–298.
[43] B. Southichak, K. Nakano, M. Nomura, N. Chiba, O. Nishimura, *Phragmites australis*: a novel biosorbent for the removal of heavy metals from aqueous solution, Water Res. 40 (2006) 2295–2302.
[44] E.W. Shin, K.G. Karthikeyan, M.A. Tshabalala, Adsorption mechanism of cadmium on juniper bark and wood, Bioresour. Technol. 98 (2007) 588–594.
[45] K. Kongolo, C. Kinabo, A. Bahr, Electrophoretic studies of the adsorption of gold and silver from aqueous cyanide solutions onto activated carbon, Hydrometallurgy 44 (1997) 191–202.
[46] A.S. Ibrado, D.W. Fuerstenau, Infrared and X-ray photoelectron spectroscopy studies on the adsorption of gold cyanide on activated carbon, Miner. Eng. 8 (1995) 441–458.
[47] S. Tunali, I. Kiran, T. Akar, Chromium(VI) biosorption characteristics of *Neurospora crassa* fungal biomass, Miner. Eng. 18 (2005) 681–689.
[48] Y.M. Pamukoglu, F. Kargi, Effects of operating parameters on kinetics of copper(II) ion biosorption onto pre-treated powdered waste sludge (PWS), Enzyme Microb. Technol. 42 (2007) 76–82.
[49] M. Jansson-Charrier, E. Guibal, J. Roussy, B. Delanghe, P. Lecloirec, Vanadium(IV) sorption by chitosan: kinetics and equilibrium, Water Res. 30 (1996) 465–475.
[50] Y. Sag, Y. Aktay, Mass transfer and equilibrium studies for the sorption of chromium ions on to chitin, Process Biochem. 36 (2000) 157–173.
[51] Z. Aksu, İ.A. İşoğlu, Removal of copper(II) ions from aqueous solution by biosorption onto agricultural waste sugar beet pulp, Process Biochem. 40 (2005) 3031–3044.
[52] M. Doğan, Y. Özdemir, M. Alkan, Adsorption kinetics and mechanism of cationic methyl violet and methylene blue dyes onto sepiolite, Dyes Pigments 75 (2007) 701–713.
[53] M.I. El-Khaiary, Kinetics and mechanism of adsorption of methylene blue from aqueous solution by nitric-acid treated water-hyacinth, J. Hazard. Mater. 147 (2007) 28–36.
[54] B.-E. Wang, Y.-Y. Hu, L. Xie, K. Peng, Biosorption behavior of azo dye by inactive CMC immobilized *Aspergillus fumigatus* beads, Bioresour. Technol. 99 (2008) 794–800.
[55] C. Gerente, P. Couespel du Mesnil, Y. Andres, J.-F. Thibault, P. Le Cloirec, Removal of metal ions from aqueous solution on low cost natural polysaccharides: sorption mechanism approach, React. Funct. Polym. 46 (2000) 135–144.
[56] D.M. Manohar, B.F. Noeline, T.S. Anirudhan, Adsorption performance of Al-pillared bentonite clay for the removal of cobalt(II) from aqueous phase, Appl. Clay Sci. 31 (2006) 194–206.
[57] E.A. Oliveira, S.F. Montanher, A.D. Andrade, J.A. Nóbrega, M.C. Rollemberg, Equilibrium studies for the sorption of chromium and nickel from aqueous solutions using raw rice bran, Process Biochem. 40 (2005) 3485–3490.
[58] S. Venkata Mohan, S.V. Ramanaiah, B. Rajkumar, P.N. Sarma, Biosorption of fluoride from aqueous phase onto algal *Spirogyra* IOI and evaluation of adsorption kinetics, Bioresour. Technol. 98 (2007) 1006–1011.
[59] Z. Gongwei, L. Zhen Liu, W. Congxiang, Flow injection analysis methods for determination of diffusion coefficients, Anal. Chim. Acta 350 (1997) 359–363.
[60] E. Ahlberg, F. Falkenberg, J.A. Manzanares, D.J. Schiffrin, Convective mass transfer to partially recessed and porous electrodes, J. Electroanal. Chem. 548 (2003) 85–94.
[61] S.R. Bai, T.E. Abraham, Biosorption of Cr(VI) from aqueous solution by *Rhizopus nigricans*, Bioresour. Technol. 79 (2001) 73–81.
[62] A. Selatnia, A. Boukazoula, N. Kechid, M.Z. Bakhti, A. Chergui, Y. Kerchich, Biosorption of lead(II) from aqueous solution by a bacterial dead *Streptomyces rimosus* biomass, Biochem. Eng. J. 19 (2004) 127–135.
[63] X.-S. Wang, Y. Qin, Removal of Ni(II), Zn(II) and Cr(VI) from aqueous solution by *Alternanthera philoxeroides* biomass, J. Hazard. Mater. 138 (2006) 582–588.